Temperature Fluctuation and Evaporative Loss Rate in an Algae Biofilm Photobioreactor

Thomas E. Murphy

Halil Berberoğlu[1]
e-mail: berberoglu@mail.utexas.edu

Mechanical Engineering Department,
Cockrell School of Engineering,
The University of Texas at Austin,
Austin, TX 78712

This study describes the thermal modeling of a novel algal biofilm photobioreactor aimed at cultivating algae for biofuel production. The thermal model is developed to assess the photobioreactor's thermal profile and evaporative water loss rate for a range of environmental parameters, including ambient air temperature, solar irradiation, relative humidity, and wind speed. First, a week-long simulation of the system has been performed using environmental data for Memphis, TN, on a typical week during the spring, summer, fall, and winter. Then, a sensitivity analysis was performed to assess the effect of each weather parameter on the temperature and evaporative loss rate of the photobioreactor. The range of the daily algae temperature variation was observed to be 12.2 °C, 13.2 °C, 11.7 °C, and 8.2 °C in the spring, summer, fall, and winter, respectively. Furthermore, without active cooling, the characteristic evaporative water loss from the system is approximately 6.0 L/m^2 day, 7.3 L/m^2 day, 3.4 L/m^2 day, and 1.0 L/m^2 day in the spring, summer, fall, and winter, respectively. [DOI: 10.1115/1.4005088]

1 Introduction

Cultivation of algae for advanced biofuel production offers a clean and sustainable alternative to fossil fuels. Traditionally, algae for biofuel production have been cultivated in open ponds or closed tubular photobioreactors (PBRs) as suspended cells, which require large volumes of water [1,2]. Recently, attached algae cell cultivation and novel biofilm photobioreactors (BPBRs) have been proposed as a platform to grow algae using less water than open pond and closed tubular photobioreactors [3,4]. The high surface area-to-volume ratio characteristic of BPBRs not only allows for efficient light harvesting and gas exchange within the BPBR but also raises significant engineering concerns such as large temperature fluctuations and elevated evaporative water loss rates.

The temperature dependence of the growth rate and of lipid productivity of a number of algal strains have been reported [5–8]. For example, the growth rate of the biofilm candidate *Botryococcus braunii* cultivated at 32 °C was twice the growth rate at 25 °C over a 2 week growth period [8]. However, over the same 2 week period, the intracellular lipid content of the *B. braunii* was 22% and 5% for the cultures cultivated at 25 °C and 32 °C, respectively.

Thus, it is of interest to understand the major modes of heat transfer in a BPBR and to predict its temperature. With the dominant modes of heat transfer understood, efficient systems can be designed to maintain optimal culture temperatures. This study presents, for the first time, the transient thermal modeling of a BPBR. Ambient air temperature, relative humidity, solar irradiation, and wind speed are the inputs of the model. The study aims to predict a characteristic temperature variation and a characteristic evaporative loss rate for a BPBR as well as to understand the dependence of these performance parameters on environmental conditions and design parameters.

2 Current State of Knowledge

To the best of our knowledge no study reports the thermal modeling of biofilm photobioreactors. Previous thermal modeling efforts concentrated on other PBR designs such as greenhouse raceway ponds, vertical flat plate PBRs, cylindrical tanks, and tubular PBRs [7,9–11]. In a study performed by Gutiérrez et al. [7], a computational heat transfer model was validated against experimental temperature data for a cylindrical tank outdoor open PBR. The tank measured 1.2 m in height and 2.4 m in diameter, and a mesh shade was used to control the amount of sunlight incident onto the culture. On a day whose ambient air temperature varied from 21 °C to 34 °C and with a maximum irradiance incident onto the tank of 300 W/m^2, the temperature of the culture varied between 25 °C and 27 °C. They indicated that the characteristic evaporative mass loss rate for this PBR was approximately 4 L/m^2 day.

Moreover, Li et al. [11] constructed and validated a thermal model of a raceway system within a greenhouse. The raceway had a depth and footprint area of 0.85 m and 280 m^2, respectively, and it was enclosed in a greenhouse with a height and footprint area of 3.5 m and 400 m^2, respectively. Given a maximum daily irradiance of approximately 750 W/m^2, the model accurately predicted a typical temperature range in the raceway water of 4 °C between night and day.

In the two aforementioned heat transfer analyses, the ratio of the illuminated surface area to the volume of the system is approximately ten times smaller than that of a BPBR. A BPBR is advantageous for energy- and cost-efficient algae production because a BPBR can be constructed inexpensively without sacrificing productivity [3,4]. Ozkan and Berberoglu [3] constructed and successfully operated a novel biofilm photobioreactor over 35 days. The authors reported that the biomass concentration reached as large as 30.7 kg/m^3, as opposed to only about 0.5 kg/m^3 observed in raceway ponds, which significantly decreases the harvesting costs. Moreover, the BPBR demonstrated an average lipid productivity of about 69.5 mg/m^2 day as opposed to a maximum of about 45 mg/m^2 day in planktonic systems [3,12]. Finally, it was estimated that the BPBR reduced the energy consumption of the system by a factor of 230 compared to a raceway pond. The biofilm photobioreactor reported by Ozkan and Berberoglu was operated at a temperature of 25 °C.

Despite the potential advantages of BPBRs for algae biofuel production, the high surface area-to-volume ratio raises concerns over the temperature variation in the algae as well as the evaporative water loss rate. With the major modes of heat transfer understood, BPBRs can be sited properly and thermal management systems can be designed and implemented. This study presents,

[1]Corresponding author.

Contributed by the Solar Energy Division of ASME for publication in the JOURNAL OF SOLAR ENERGY ENGINEERING. Manuscript received May 11, 2011; final manuscript received September 1, 2011; published online November 1, 2011. Assoc. Editor: Wojciech Lipinski.

for the first time, a thermal analysis of a BPBR to predict the algae biofilm temperature and evaporative loss rate.

3 Analysis

Consider a planar algae BPBR featuring a length L of 10 m as shown in Fig. 1(*a*). A photograph of a prototype BPBR used in our laboratory is also shown in Fig. 1(*b*). Due to the symmetry of the system, this analysis was performed for unit depth into the page. The BPBR consists of a horizontal concrete layer of thickness $t_c = 0.05$ m in direct contact with the ground, an algae biofilm layer of thickness $t_a = 0.005$ m on top of the concrete layer, and a water layer on top of the algae layer of thickness $t_w = 0.05$ m. The bulk water velocity parallel to the algae surface is v_w, which is equal to 0.05 m/s. These parameters were selected due to their similarity to the parameters of the system designed by Ozkan and Berberoglu that had a lipid productivity of 69.5 mg/m^2 day. The system is illuminated by direct sunlight $G_{\text{sun}}(\tau)$, whose irradiance is a function of the hour of the day and the day of the year, as well as location. The system is exposed to ambient air at temperature T_{air}, relative humidity ϕ_{air}, and wind velocity v_{air}. The ground below the concrete had the thermal properties of soil as reported in Ref. [13].

3.1 Assumptions. In order to make the problem mathematically tractable it is assumed that: (1) the thermal conductivity of the algae biofilm is isotropic as the cells are spherical and there is no preferential directionality in the structure of the biofilm, (2) thermal properties of air, water, algae, concrete, and ground were assumed to be constant and evaluated at 300 K, and (3) thermal conductivity, specific heat, and mass density of the algae are equal to the respective properties for water as algae are 90% water by mass [4]. The remaining 10% of algal mass is predominantly protein, carbohydrates, and lipids [14]. This chemical composition is similar to that of banana. A banana with 75% water content has a thermal conductivity, specific heat, and mass density that are

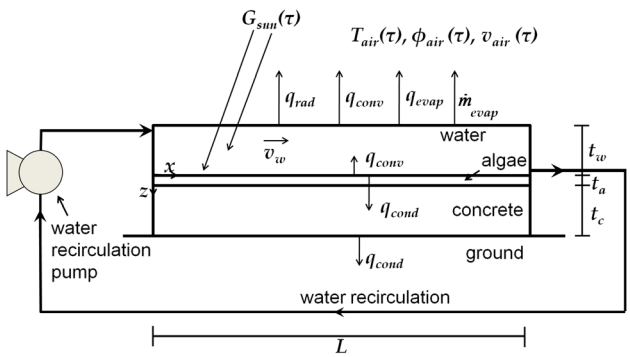

(a)

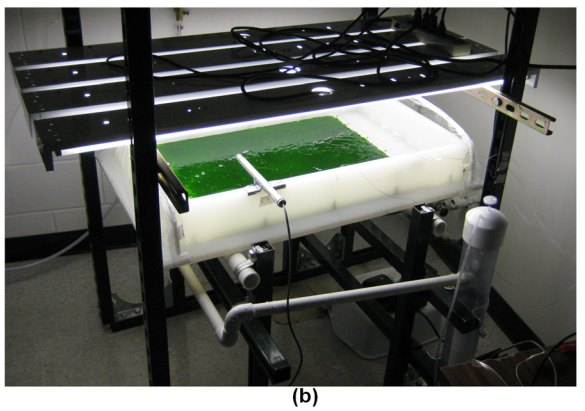

(b)

Fig. 1 (*a*) Schematic of the geometry and heat transfer processes of the system and (*b*) photograph of the prototype biofilm photobioreactor in our laboratory

78%, 80%, and 98% of those respective properties in pure water [13]. Therefore, modeling the algae, that is, 90% water as pure water will probably cause an overestimate in its thermal conductivity and specific heat by less than 10% and have a negligible error on mass density. It is further assumed that (4) Beer's law can be applied to estimate the light profile in the biofilm and the water, (5) algae have a photosynthetic efficiency of 10%, i.e., 10% of the solar radiation is utilized in biochemical reactions, while the rest of the energy is dissipated as heat [15], (6) the spectral reflectivity of the algae is equal to the spectral reflectivity for green pine needles [16], and (7) air behaves as an ideal gas. Furthermore, due to the relatively larger thickness of the turbulent mixing layer compared to that of the boundary layer, the water layer is treated as isothermal in z direction.

3.2 Heat Transfer in the Water Layer. The flowing water layer on top of the algae biofilm was discretized in the direction of flow into nodes of depth t_w and length Δx, and a control volume energy analysis was performed on each node. Each node was heated by solar irradiation. Each node also experienced evaporative cooling with the air surrounding it, and convection heat transfer with the air as well as with the algae biofilm on the bottom. Finally, the water emitted thermal radiation to the sky.

A spectral analysis was performed to determine the rate of heating of each water node by solar radiation. The solar spectrum used was the direct normal and circumsolar spectrum provided by the National Renewable Energy Laboratories (NREL) with a spectral resolution of 1 nm [17]. The spectral absorption coefficients of water a_λ were obtained from the discussion in Ref. [18]. The Beer–Lambert law was applied to determine the spectral irradiance for every wavelength at the non-light-facing side of the water layer [19]

$$G_\lambda(t_w) = G_{o,\lambda} e^{-a_\lambda t_w} \tag{1}$$

where $G_{o,\lambda}$ is the spectral irradiance at wavelength λ at the light-facing surface of the water layer, in W/m^{2}nm.

The rate of solar heating of each node was then calculated by

$$q_{w,\text{rad}} = \left[\sum_{\lambda=0}^{\infty} \left[G_{o,\lambda}(0) - G_\lambda(t_w)\right]\Delta\lambda\right]\Delta x \tag{2}$$

where $\Delta\lambda$ is the wavelength range around λ, which was 1 nm due to the resolution of the solar spectrum used for analysis.

The rate of convection heat transfer between each node and the air is given by Newton's law of cooling [13]

$$q_{\text{conv},w\to\text{air}} = \bar{h}_{w\to\text{air}}(T_w(x) - T_{\text{air}})\Delta x \tag{3}$$

where $T_w(x)$ and T_{air} are the local water and air temperatures in K and $\bar{h}_{w\to\text{air}}$ is the average convection coefficient between water and air in W/m^2 K. The latter was determined from the Nusselt number according to [13]

$$\overline{\text{Nu}}_{w\to\text{air}} = \frac{\bar{h}_{w\to\text{air}} L}{k_{\text{air}}} \tag{4}$$

where L is the characteristic length of the system, equal to 10 m, and k_{air} is the thermal conductivity of air in W/mK. For the mixed natural and forced convection conditions that exist at the air-water interface, the Nusselt number is calculated using the correlation suggested by Mills [20]

$$\overline{\text{Nu}}^{7/2}_{w\to\text{air}} = \overline{\text{Nu}}^{7/2}_{w\to\text{air,nat}} + \overline{\text{Nu}}^{7/2}_{w\to\text{air,for}} \tag{5}$$

where $\overline{\text{Nu}}_{w\to\text{air,for}}$ is the Nusselt number for forced convection and is given by [13],

$$\overline{\mathrm{Nu}}_{w\to\mathrm{air,for}} = 0.664\mathrm{Re}_{\mathrm{air}}(L)^{1/2}\mathrm{Pr}_{\mathrm{air}}^{1/3} \tag{6}$$

where $\mathrm{Re}_{\mathrm{air}}(L)$ is the Reynolds number of the air flow above the water layer based on the wind velocity v_{air} and the characteristic length scale L, and $\mathrm{Pr}_{\mathrm{air}}$ is the Prandtl number of air at 300 K, equal to 0.7. In Eq. (5), the Nusselt number of the natural convection $\overline{\mathrm{Nu}}_{w\to\mathrm{air,nat}}$ is calculated by the correlation [13]

$$\overline{\mathrm{Nu}}_{w\to\mathrm{air,nat}} = C\mathrm{Ra}_{\mathrm{air}}^{n} \tag{7}$$

where the values of C and n are equal to 0.15 and 1/3, respectively, if the water is warmer than the air (buoyancy-aided convection), whereas these two constants are equal to 0.27 and 1/4, respectively, if the water is colder than the air (buoyancy-inhibited convection). $\mathrm{Ra}_{\mathrm{air}}$ is the Rayleigh number at the air–water interface, defined as [13]

$$\mathrm{Ra}_{\mathrm{air}} = \frac{g\beta_{\mathrm{air}}|T_{\mathrm{air}} - T_w|L^3}{\nu_{\mathrm{air}}\alpha_{\mathrm{air}}} \tag{8}$$

where g is the acceleration due to gravity, equal to 9.8 m/s^2, β_{air} is the thermal expansion coefficient of air, equal to $1/T_{\mathrm{film}}$ for an ideal gas, ν_{air} is the kinematic viscosity of air in m^2/s, and α_{air} is the thermal diffusivity of air in m^2/s.

Furthermore, the rate of evaporative cooling of the water is calculated according to [21]

$$q_{\mathrm{evap}}(x) = \dot{m}_{\mathrm{evap}}(x)h_{fg} \tag{9}$$

where h_{fg} is the latent heat of vaporization of water in J/kg and $\dot{m}_{\mathrm{evap}}(x)$ is the local evaporative loss rate in kg/s and is calculated by [21]

$$\dot{m}_{\mathrm{evap}} = g_{m,w\to\mathrm{air}}(\omega_w - \omega_{\mathrm{air}})\Delta x \tag{10}$$

where $g_{m,w\to\mathrm{air}}$ is the mass transfer coefficient in kg/m^{2}s and ω_w and ω_{air} are the mass fractions of water vapor in air at the air-water interface and in the ambient air, respectively. The water mass fractions ω are calculated by [22]

$$\omega = 0.622\frac{p_w(T)}{p_{\mathrm{atm}} - p_w(T)} \tag{11}$$

where $p_w(T)$ is the partial pressure of water vapor. For the water mass fraction at the air–water interface ω_w, p_w is equal to the saturation pressure of water at temperature T_w, whereas for ω_{air}, p_w is equal to the saturation pressure of water at temperature T_{air} times the relative humidity ϕ_{air}.

The mass transfer coefficient $g_{m,w\to\mathrm{air}}$ is given by [21]

$$g_{m,w\to\mathrm{air}} = \frac{\rho_{\mathrm{air}}D_{w,\mathrm{air}}}{\mathrm{Sh}_{\mathrm{air}}L} \tag{12}$$

where ρ_{air} is the mass density of air in kg/m^3, $D_{w,\mathrm{air}}$ is the binary diffusion coefficient of water vapor in air at 300 K, equal to 2.6×10^{-5} m^2/s, and $\mathrm{Sh}_{\mathrm{air}}$ is the Sherwood number of the mass transfer. The Sherwood number is calculated in an analogous way to calculating the Nusselt number in Eqs. (6) and (7), but by using the Schmidt number instead of the Prandtl number [21]. The Schmidt number for water in air is 0.55 [21].

Moreover, the rate of heat transfer from the top layer of the algae surface to the water at a given downstream distance x was determined by Newton's law of cooling [13]

$$q_{a\to w}(x) = h_w(x)(T_a(x, y=0) - T_w(x))\Delta x \tag{13}$$

where $T_a(x, y=0)$ is the biofilm temperature at the biofilm-water interface at downstream location x and $T_w(x)$ is the water temperature at downstream location x. The Nusselt number for the turbulent flow was calculated by [13]

$$\mathrm{Nu}_{a\to w}(x) = 0.0296\mathrm{Re}_w(x)^{4/5}\mathrm{Pr}_w^{1/3} \tag{14}$$

A turbulent boundary layer between the algae and water was assumed because of the high degree of free stream turbulence caused by the drip system at the entry.

Moreover, the heat lost from each water node by radiation was calculated as

$$q_{w,\mathrm{rad}} = \epsilon\sigma\left(T_w^4 - T_{\mathrm{sky}}^4\right)\Delta x \tag{15}$$

where σ is the Stefan–Boltzmann constant equal to 5.67×10^{-8} W/m^2 K^4, ϵ is the total hemispherical emissivity of water, equal to 0.93 [19], and T_{sky} is calculated by [23]

$$T_{\mathrm{sky}} = T_{\mathrm{air}}\left[0.71 + 0.0056T_{dp} + 7.3\times10^{-5}T_{dp}^2 + 0.013\cos(15m)\right]^{1/4} \tag{16}$$

where T_{dp} is the dew point temperature in degrees Celsius and m is the hour from midnight.

The net heat transfer into the ith node due to enthalpy flow was calculated by

$$q_{w,\mathrm{flow}} = \rho_w t_w v_w c_w\left(T_{w,i-1} - T_{w,i}\right) \tag{17}$$

where ρ is the density of water in kg/m^3, v_w is the water velocity in m/s, and c_w is the specific heat of water in J/kgK.

3.3 Heat Transfer in the Algae Biofilm. The algae biofilm was discretized into nodes of length Δx equal to the length of each water layer node and thickness Δz_a. The nodes adjacent to the water layer experienced heating by solar irradiation, convection with the water layer, and conduction into the algae node below and on each side. Thermal radiation loss from the algae was not taken into account as the water layer above it was opaque at long wavelength radiation, and the temperature difference between the algae and the water was not large enough for significant thermal radiation exchange. The bottom nodes experienced conduction heat transfer with the nodes above, on each side, and with the adjacent concrete node below, as well as heating by solar irradiation. All other nodes within the algae biofilm experienced conduction heat transfer with adjacent nodes and heating by solar irradiation.

The rate of heating by solar radiation for algae nodes located at a distance of i nodes from the light-facing surface of the algae (the ith node) was calculated by

$$q_{\mathrm{abs},i} = \left(G_{in} - G_{\mathrm{abs},w}\right)(1 - r_a)\left(1 - \eta_{ph}\right)\left[e^{-X_aA_a(i-1)\Delta z_a} - e^{-X_aA_ai\Delta z_a}\right]\Delta x \tag{18}$$

where G_{in} is the radiation incident onto the water layer, $G_{\mathrm{abs},w}$ is the radiation absorbed by the water, r_a is the total reflectivity of the algae based on the analysis provided by Williams [16], η_{ph} is the photosynthetic efficiency of the algae, assumed to be 10%, X_a is the mass concentration of algae in the biofilm, approximated as 30 kg/m^3 based on the results presented by Ozkan and Berberoglu [3], and A_a is the mass absorption cross section averaged over the spectral region of irradiance for *Chlamydomonas reinhardtii*, equal to 125 m^2/kg based on the analysis by Berberoglu et al. [24].

The net rate of heat transfer into the (i, j) node by conduction is given by Fourier's Law for discretized volumes [13]

$$q_{\mathrm{cond,net}} = k_a\frac{T_{i-1} - 2T_i + T_{i+1}}{\Delta z_a}\Delta x + k_a\frac{T_{j-1} - 2T_j + T_{j+1}}{\Delta x}\Delta z_a \tag{19}$$

where the first term is the net rate of conduction heat transfer in the z direction and the second term is the net rate of conduction heat transfer in the x direction.

3.4 Heat Transfer in the Concrete and Ground. The concrete layer was discretized into nodes with length Δx and thickness Δz_c. The top and bottom nodes experienced conduction with the bottom algae nodes and the top ground nodes, respectively, as well as conduction with the node on each side. Each other node experienced conduction with the nodes above and below and on each side. The ground was modeled as soil 1 m deep and discretized into nodes of length Δx and thickness Δz_g. The thermal penetration depth into the ground was shown to be less than 1 m. Each ground node experienced conduction with adjacent nodes. Net heat flux by conduction in each node in the concrete and ground was calculated using Eq. (19) using each material's respective conductivity k.

3.5 Closure Laws and Weather Parameters. Thermal and fluid properties of air, water, algae, concrete, and ground were evaluated at 300 K and are shown in Table 1. Four week-long simulations using weather parameters for the spring, summer, fall, and winter were performed for Memphis, TN. Memphis was selected because its moderately high annual insolation, proximity to water sources, high average relative humidity, and moderate temperatures make it a viable candidate as a location for commercial algae production. The spring, summer, fall, and winter weeks were May 12–18, July 7–13, September 26–October 2, and November 28–December 4, 2010. The values for hourly air temperature, irradiance, relative humidity, and wind speed were obtained from the National Renewable Energy Laboratory's *Typical Meteorological Year 3* data set, which reports real weather data that was deemed typical of the time span 1991–2005 [25]. The weather parameters used are shown in Fig. 2.

Moreover, to assess the importance of each weather parameter on the algae biofilm temperature and evaporative loss rate, a sensitivity analysis was conducted using the spring week as a base case. The values of ambient temperature in degrees Celsius, irradiance, relative humidity, and wind speed were each independently increased and decreased by 10% and 20% compared to their base case value while holding the other weather parameters at their base case values.

3.6 Boundary and Initial Conditions. The initial temperature of the system, which included the water, algae, and concrete, was set to 23 °C, 28 °C, 20 °C, and 8 °C for the spring, summer, fall, and winter simulations, respectively. The temperature deep within the ground at a given geographic location is approximately equal to that location's annual average air temperature [20]. Therefore, the initial temperature for the ground varied linearly in z between the initial temperature of the system and the temperature deep within the ground, which was 17 °C [25]. A convection boundary condition was imposed at each edge of the algae biofilm, i.e., where x was equal to zero and where x was equal to L, using the convection coefficient $h_{a\rightarrow w}$ at each location calculated by Eq. (14). The water recirculation pipe, as well as each edge of the concrete and ground layers, was assumed to be perfectly insulated.

3.7 Solution Procedure. A fully explicit time stepping method was used by which the temperature change of a node between consecutive time steps was calculated from the net energy flux into the node and the heat capacity of the node. A custom MATLAB code was written to implement this method. A grid sensitivity analysis was performed in both spatial and temporal discretization to ensure grid size independence of the results. The time discretization was varied from 0.01 to 1 s, the discretization in x was varied from 38 mm to 2000 mm, and the discretization in the algae layer z_a was varied from 0.25 mm to 1 mm. The results indicated that the discrepancy between the temperatures predicted by any two discretizations never exceeded 0.1%, and, therefore, the model is independent of temporal and spatial discretization. In order to decrease computing time, a highly skewed spatial discretization was used wherein algae layer nodes had an aspect ratio of 1000. This is justified because the difference in algae temperatures between the spatial discretizations with aspect ratios of 1000 and 40 was less than 0.1%.

Table 1 Thermal properties of materials at 300 K [13]

Material	k (W/mK)	c (kJ/kgK)	ρ (kg/m^3)
Air	0.026	1.0	1.16
Water	0.61	4.2	1000
Algae	0.61	4.2	1000
Concrete	1.0	0.75	2400
Soil	0.52	1.8	2050

4 Results and Discussion

4.1 Temperatures and Evaporation During the Week Simulations

4.1.1 Spring. Figure 3(*a*) (top) shows the maximum and minimum algae temperatures as a function of time during the week of May 12–18. The ambient air temperature is also shown for comparison. The maximum daily algae temperature occurs at approximately 2:00 PM each day, whereas the maximum solar irradiance occurs at noon. The maximum daily algae temperature exceeded the maximum daily air temperature by an average of 1.9 °C over the week as a result of solar heating. The difference between the minimum algae temperature and the air temperature at night was a strong function of the nightly relative humidity. On the second and third nights of the simulation (from hours 18–30 and 42–54), the average relative humidity was approximately 89%. As a result, the rate of evaporative cooling was slow and the algae temperature was approximately equal to the air temperature. On the other hand, on the fifth and sixth nights (from hours 92–104 and 116–128), the average relative humidity was only 61%. As a result, evaporative cooling was fast, and the algae temperature was, an average, 2.0 °C less than the ambient air temperature. The average daily algae temperature range over the course of the week was 12.2 °C, whereas the daily range of air temperatures was only 9.6 °C.

Figure 3(*a*) (bottom) shows the hourly evaporative water loss over the course of the week. The figure indicates that the rate of water loss is strongly correlated with the algae temperature. The maximum hourly evaporative loss rate is approximately 0.7 L/m^2 h, and it occurs at approximately the same time as does the maximum algae temperature, whereas the evaporative loss rate is an order of magnitude slower at night. Therefore, strategies to minimize temperature fluctuations in BPBRs can also be used to mitigate evaporative losses. The characteristic daily evaporative water loss for this week is approximately 6.0 L/m^2 day.

4.1.2 Summer. Figure 3(*b*) (top) shows the maximum and minimum algae temperatures as a function of time during the summer week of July 7–13. In the summer week, the maximum algae temperature exceeded the maximum air temperature by an average of 1.5 °C. This difference was less than the difference in the spring (1.9 °C) because the warmer water temperatures in the summer caused an increase in the rate of evaporative cooling. The minimum nightly algae temperatures were an average approximately 1.7 °C cooler than the minimum nightly air temperatures. The average daily temperature range over the course of the week was 13.2 °C for the algae, compared with 10.0 °C for the ambient air. Averaged over the week, the maximum hourly evaporative loss rate was approximately 0.8 L/m^2 h and it occurred at approximately the same time as the maximum algae temperature (Fig. 3(*b*) (bottom)). The characteristic daily evaporative loss was 7.3 L/m^2 day.

4.1.3 Fall. During the week of September 26–October 2, the algae temperature very closely followed the ambient air

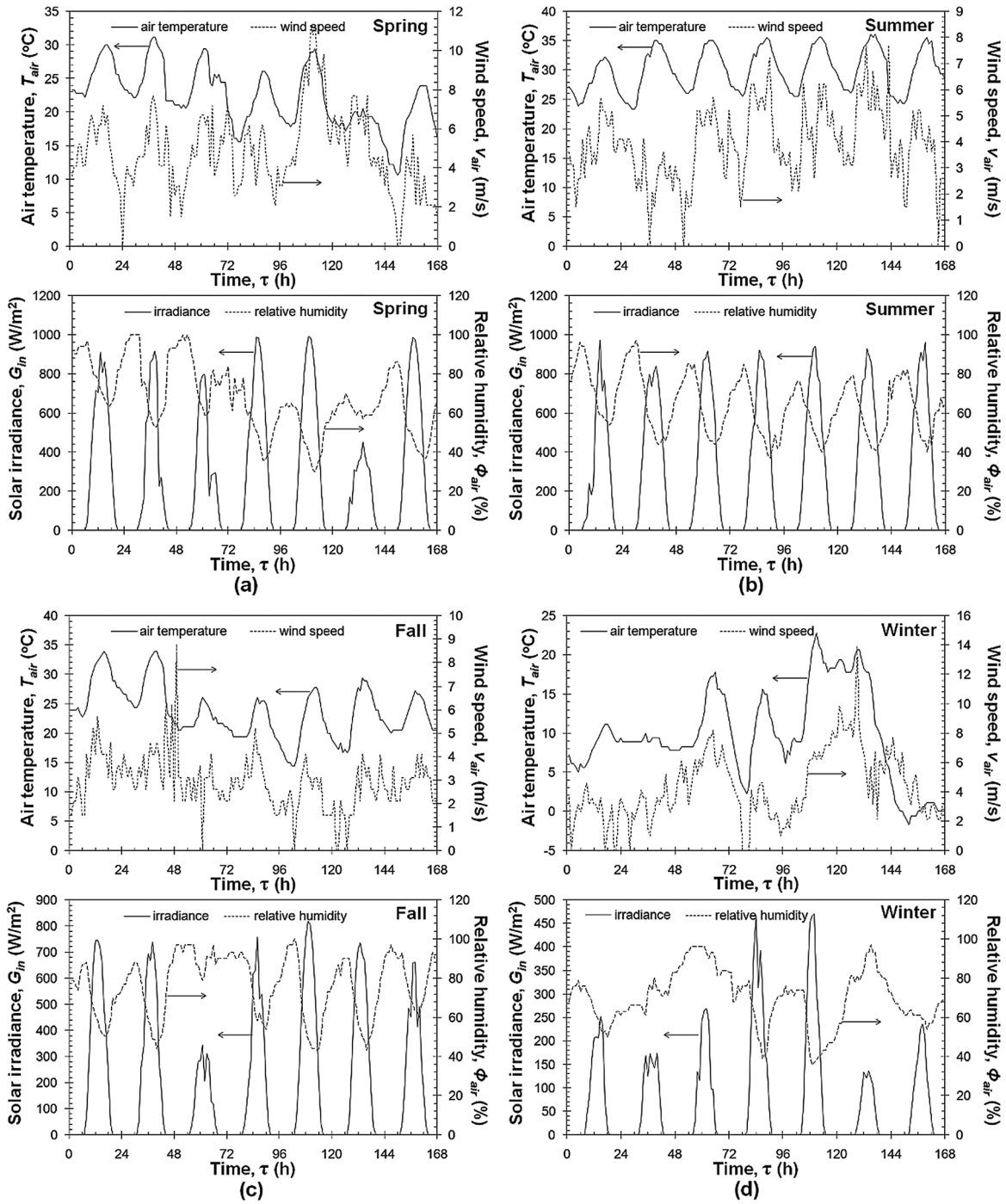

Fig. 2 Hourly air temperature, wind velocity, solar irradiance, and relative humidity for: (*a*) the spring week of May 12–18, (*b*) the summer week of July 7–13, (*c*) the fall week of September 26–October 2, and (*d*) the winter week of November 28–December 4 for Memphis, TN

temperature due to a balance between the rate of solar heating and the rate of evaporative cooling (Fig. 3(*c*)). The average daily temperature range in the algae during this week was 11.7 °C, compared to a 10.0 °C temperature range in the ambient air. Condensation onto the system was observed during several time periods of this week, as shown by the negative evaporation rate. The characteristic daily evaporative loss rate was 3.4 L/m^2 day.

4.1.4 Winter. Figure 3(*d*) (top) shows the maximum and minimum algae temperatures over the course of the week of November 28–December 3. The results for December 4 are not shown because the algae temperature dropped below zero degrees Celsius, and the numerical model is not equipped to predict phenomena associated with freezing. During this week, the rate of solar heating was an average only 250 W/m^2 and as a result, the maximum algae temperature during the day is, an average, 2.5 °C colder than the maximum air temperature. The average daily temperature range in the algae was 8.2 °C, compared to a daily range of air temperatures of 9.9 °C. The hourly evaporation profile shown in Fig. 3(*d*) (bottom) indicates that condensation was also observed during this week. The characteristic daily water loss for this winter week was 1.0 L/m^2 day. Table 2 summarizes the seasonal variation of temperature fluctuation and evaporative loss.

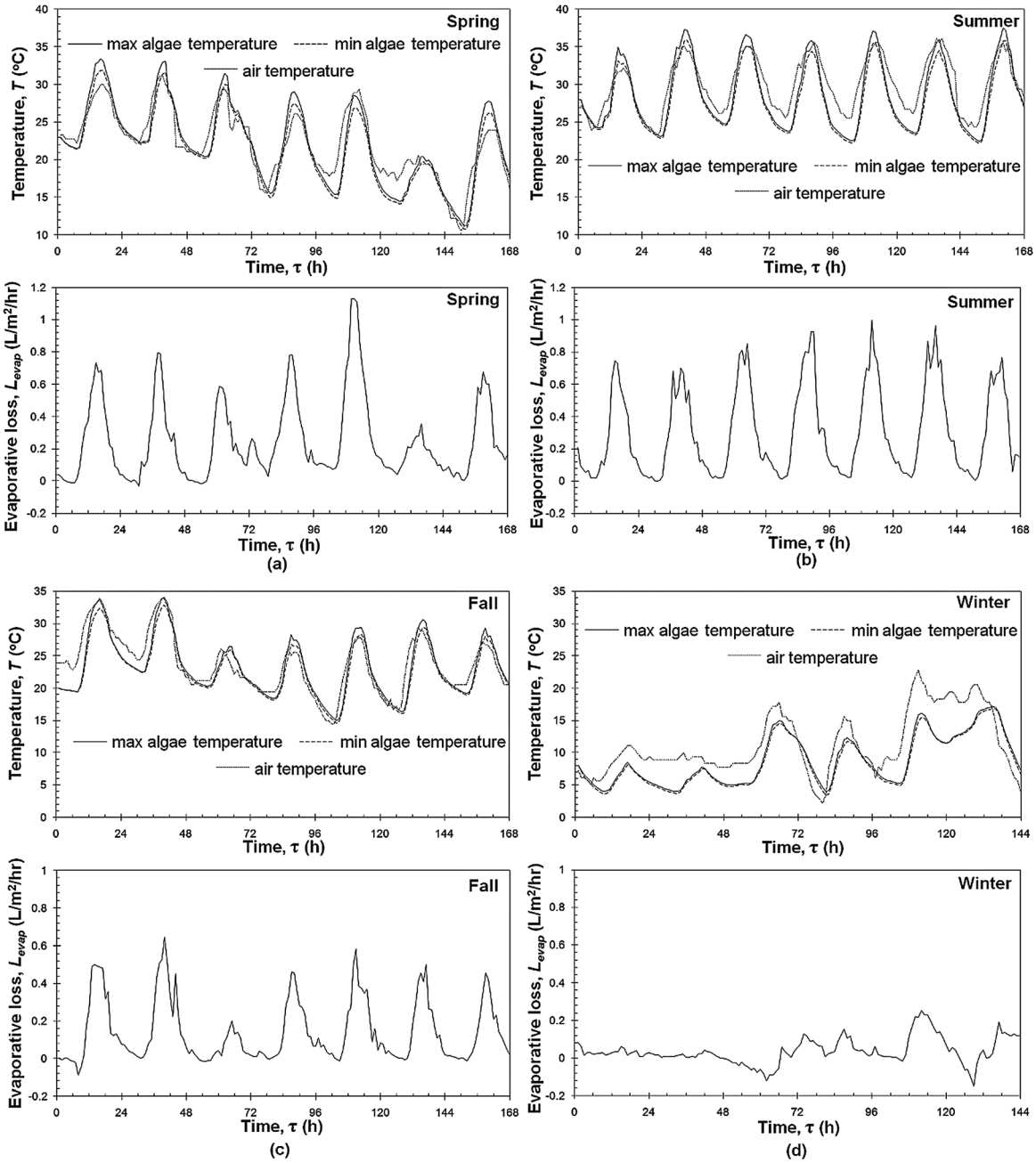

Fig. 3 Algae biofilm temperatures and evaporative loss rates for: (*a*) spring, (*b*) summer, (*c*) fall, and (*d*) winter. On the temperature plots, solid lines represent the maximum algae temperature in the biofilm, dashed lines represent the minimum algae temperature in the biofilm, and the dotted lines represent the ambient air temperature.

Table 2 Summary of seasonal dependence of temperature fluctuation and evaporation rate

	Spring	Summer	Fall	Winter
Average air temperature $\bar{T}_{\text{air}}$ (°C)	22.2	30.0	23.8	9.7
Average daily air temperature range $\overline{\Delta T}_{\text{air}}$ (°C)	9.6	10.0	10.0	9.9
Average algae temperature $\bar{T}_a$ (°C)	21.8	28.4	23.1	7.6
Average daily algae temperature range $\overline{\Delta T}_a$ (°C)	12.2	13.2	11.7	8.2
Average Evaporative rate $\bar{L}_{\text{evap}}$ (L/m^2 day)	6.0	7.3	3.4	1.0

4.2 Sensitivity Analysis. Figure 4(*a*) shows the percent deviation in maximum daily algae temperature on May 13 as a function of the variation of each weather parameter. Increasing the average air temperature, irradiance, and relative humidity by 10% increase the maximum daily algae temperature by 6.8%, 3.9%, and 3.7%, respectively. Increasing the average wind velocity by 10% decreases the maximum temperature by 0.3%. Increasing the irradiance causes an increase in maximum algae temperature by increasing the daily solar heating, whereas increasing the relative humidity increases the maximum temperature by decreasing the rate of evaporative cooling. Increasing the wind velocity increases the rate of evaporative cooling.

Furthermore, Fig. 4(*b*) shows the percent deviation in minimum daily algae temperature on May 13 as a function of the variation of each environmental parameter. Increasing the average air temperature and relative humidity by 10% increases the minimum daily

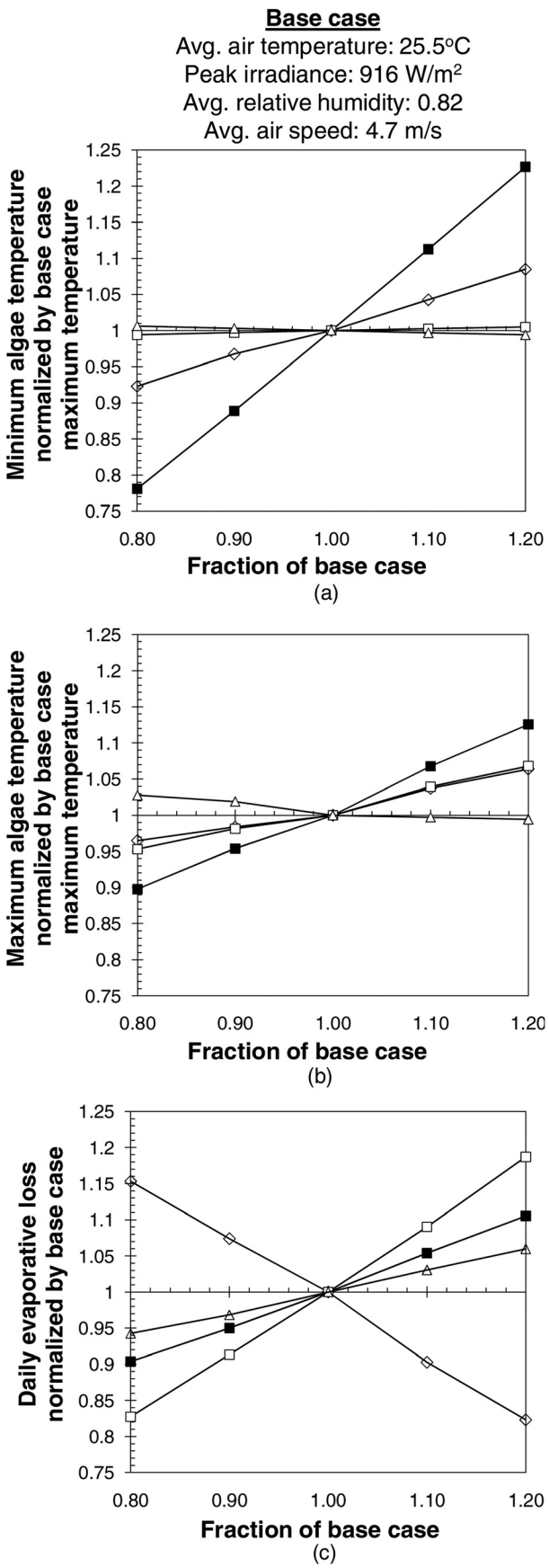

Fig. 4 Relative sensitivities of (*a*) maximum and (*b*) minimum daily algae temperature and (*c*) evaporative loss rate to changes in air temperature in °C (■), relative humidity (◊), irradiance (□), and wind velocity (Δ)

algae temperature by 8.6% and 4.3%, respectively. Increasing the average wind velocity by 10% decreases the minimum temperature by 0.3% and increasing the irradiance by 10% has a negligible effect on the minimum temperature. These results indicate that increasing the average air temperature and the relative humidity increase the algae temperature at all locations in the biofilm at all times. Increasing the wind velocity has the opposite effect, decreasing the algae temperature at all times and all locations due to the increase in the rate of evaporative cooling. Increasing the irradiance increases the algae temperature at all locations during the day but has no effect on the temperatures at night.

Finally, Fig. 4(*c*) shows the effect of varying each weather parameter on the total daily evaporative water loss. Increasing the irradiance, air temperature, and wind speed by 10% increases the daily evaporative water loss by 9.0%, 5.4%, and 3.1%, respectively. Increasing the relative humidity by 10% has the opposite effect, decreasing the evaporative loss by 9.7%.

4.3 Varying the Water Layer Depth for Temperature Stabilization. The effects of varying the water layer depth between 0.01 m and 0.1 m on algae temperature and evaporative loss rate were also investigated, and the results are shown in Fig. 5. The figure shows output data using the weather parameters of

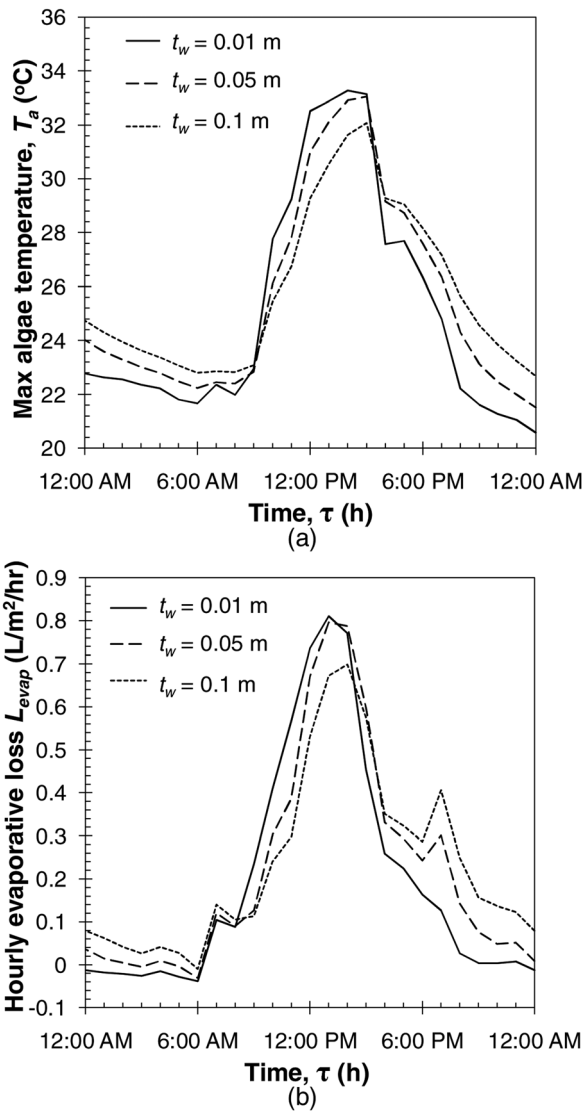

Fig. 5 Maximum algae temperature and evaporative loss rate for BPBRs with water layer thicknesses varying from 0.01 m to 0.1 m on May 13

May 13. It indicates that increasing the thickness of the water layer (i) decreases the amplitude of the daily temperature oscillation and (ii) slows the temporal response of the system such that the maximum algae temperature occurs later in the day. For a water layer thicknesses of 0.01 m and 0.1 m, the maximum algae temperatures are 33.3 °C and 32.1 °C, respectively, and they occur at approximately 2:00 PM and 3:00 PM, respectively. Furthermore, increasing the water layer thickness causes the algae to stay warmer after the sun goes down due to the increased thermal inertia of the system. As a result, the evaporative loss rate for the system with a 0.1 m thick water layer is less than that with the 0.01 m water layer between the hours 8:00 AM and 2:00 PM, whereas at all other hours the evaporative loss rate of the system with the 0.1 m thick water layer is greater than that of the system with the 0.01 m layer. As a result, the total daily evaporative water loss increases slightly with increasing water layer thickness: the total daily evaporative loss for the systems with the water layer thicknesses of 0.01 m, 0.05 m, and 0.1 m were 4.8, 5.4, and 5.7 L/m^2 day, respectively. The evaporative loss was shown to further decrease to 4.4 L/m^2 day for a water layer thickness of 0.001 m.

4.4 Implications of Temperature Fluctuations on Biofilm Productivity. The cultivation temperature of photosynthetic biofilms has a significant effect on its growth and product formation rates [5–8]. For example, the green alga *B. braunii* and the photosynthetic bacteria *Rhodopseudomonas palustris* demonstrated maximum growth and hydrogen production rates at 32 °C and 25 °C, respectively, and these rates decreased by as much as 34% when the cultivation temperature was increased or decreased by 10 °C [6,8]. Coupled with detailed data on the growth and product formation rates of a given species as a function of temperature, the model presented here enables optimal siting of BPBRs and prediction of temporally dependent growth and product formation rates. Furthermore, this model enables the virtual testing of thermal management strategies to control biofilm temperature for maximum productivity.

5 Conclusions

The goal of this study was to create a numerical finite volume model to quantify the temperature variation and the evaporative water loss characteristic of an algae biofilm photobioreactor. First, the maximum and minimum algae temperatures and the evaporative loss rate were determined during 1 week periods in the spring, summer, fall, and winter for Memphis, TN. Second, a sensitivity analysis was performed to determine the relative effects of ambient air temperature, irradiance, relative humidity, and wind speed on the algae temperature and evaporative loss rate. Finally, the effects of varying the thickness of the water layer flowing over the algae biofilm were investigated. Based on the results obtained in the study, the following conclusions can be drawn:

- For the spring, summer, fall, and winter simulations, the average daily algae temperature ranges were 12.2 °C, 13.2 °C, 11.7 °C, and 8.2 °C, respectively. By comparison, the average air temperature ranges for these simulations were 9.6 °C, 10.0 °C, 10.0 °C, and 9.9 °C, respectively.
- The average evaporative water loss rates of the system in the spring, summer, fall, and winter simulations were approximately 6.0 L/m^2 day, 7.3 L/m^2 day, 3.4 L/m^2 day, and 1.0 L/m^2 day, respectively.
- Compared to the base case week with an average air temperature of 22 °C, an average relative humidity of 67%, an average peak daily irradiance of 830 W/m^2, and an average wind speed of 4.8 m/s, a 10% increase in the average air temperature and a 10% decrease in relative humidity increased the algae temperature at all times by approximately 7.7% and 4.0%, respectively. A 10% increase in irradiance increased the average daily algae temperature by 3.9% but did not affect the algae temperature at night. A 10% increase in wind speed decreased the algae temperature at all times by approximately 0.3%.
- For water layer thicknesses of 0.01 m and 0.1 m, the maximum algae temperatures on May 13 were 33.3 °C and 32.1 °C, respectively. Increasing the water layer thickness from 0.01 m to 0.1 m caused the maximum evaporation rate to occur later in the day and increased the daily evaporative loss by approximately 18%.

This model, along with the sensitivity analysis associated with it, allows biofilm photobioreactor designers to estimate algae temperatures and evaporative loss rates given weather parameters for a given time of year and geographic location. Coupled with detailed knowledge of the effect of cultivation temperature on growth and product formation rates, this model can aid in designing thermal management strategies for maximum productivity. Finally, the results can be improved by experimentally measuring the thermal and radiative properties of algae biofilms and integrating these closure laws into the modeling framework described in this study.

Nomenclature

a = absorption coefficient, 1/m
c = specific heat at constant pressure, J/kgK
D = mass diffusivity, m^2/s
G = irradiance, W/m^2
g = acceleration due to gravity, m/s^2
g_m = mass transfer coefficient, kg/m^{2}s
h = convection coefficient, W/m^{2}K
h_{fg} = enthalpy of vaporization, J/kg
k = thermal conductivity, W/mK
L = length of the photobioreactor, m
m = hour from midnight
$\dot{m}$ = rate of mass evaporation, kg/s
Nu = Nusselt number
p = partial pressure, Pa
Pr = Prandtl number
q = rate of heat transfer, W
Ra = Rayleigh number
Re = Reynolds number
Sh = Sherwood number
T = temperature, K
t = thickness of layer, m
v = velocity, m/s

Greek Symbols

α = thermal diffusivity, m^2/s
β = thermal expansion coefficient, 1/K
ϕ = relative humidity
λ = wavelength, nm
ν = kinematic viscosity, m^2/s
ρ = density, kg/m^3
τ = time, s

Subscripts

a = refers to algae
abs = refers to absorption
air = refers to air
atm = refers to atmospheric
c = refers to concrete
cond = refers to conduction
conv = refers to convection
dp = refers to dew point
evap = refers to evaporation
for = refers to forced convection

in = refers to incident
g = refers to ground
nat = refers to natural convection
rad = refers to radiation
sat = refers to saturation
w = refers to water

References

[1] Molina Grima, E., Acien Fernandez, F., Garcia Camacho, F., and Chisti, Y., 1999, "Photobioreactors: Light Regime, Mass Transfer, and Scaleup," J. Biotechnol., **70**, pp. 231–247.
[2] Suh, S., and Lee, C., 2003, "Photobioreactor Engineering: Design and Performance," Biotechnol. Bioprocess Eng., **8**, pp. 313–321.
[3] Ozkan, A., and Berberoglu, H., 2010, "Novel Biofilm Photobioreactor for Minimizing Energy and Water Requirements of Algae Cultivation," ASME International Mechanical Congress and Exposition, IMECE2010-39621.
[4] Johnson, M., and Wen, Z., 2009, "Development of an Attached Microalgal Growth System for Biofuel Production," Appl. Microbiol. Biotechnol., **85**(3), pp. 525–534.
[5] Weiss, V., Gromet-Elhanan, Z., and Halmann, M., 1985, "Batch and Continuous Culture Experiments on Nutrient Limitations and Temperature Effects in the Marine Alga *Tetraselmis suecica*," Water Res., **19**(2), pp. 185–190.
[6] Tian, X., Liao, Q., Zhu, X., Wang, Y., Zhang, P., Li, J., and Wang, H., 2010, "Characteristics of a Biofilm Photobioreactor as Applied to Photo-Hydrogen Production," Bioresour. Technol., **101**(3), pp. 977–983.
[7] Gutiérrez, J., Porta-Gándara, M., and Fernández, J., 2008, "Passive Temperature Solar Control of an Outdoor Photobioreactor," Renewable Energy, **33**(8), pp. 1892–1903.
[8] Kalacheva, G. S., Zhila, N. O., Volova, T. G., and Gladyshev, M. I., 2002, "The Effect of Temperature on the Lipid Composition of the Green Alga Botryococcus," Microbiology, **71**(3), pp. 286–293.
[9] Sierra, E., Acién, F., Fernández, J., García, J., González, C., and Molina, E., 2008, "Characterization of a Flat Plate Photobioreactor for the Production of Microalgae," Chem. Eng. J., **138**(1–3), pp. 136–147.
[10] Morita, M., Watanabe, Y., and Saiki, H., 2001, "Evaluation of Photobioreactor Heat Balance for Predicting Changes in Culture Medium Temperature Due to Light Irradiation," Biotechnol. Bioeng., **74**(6), pp. 466–475.
[11] Li, S., Willits, D., Browdy, C., Timmons, M., and Losordo, T., 2009, "Thermal Modeling of Greenhouse Aquaculture Raceway Systems," Aquacultural Eng., **41**, pp. 1–13.
[12] Mata, T. M., Martins, A. A., and Caetano, N. S., 2010, "Microalgae for Biodiesel Production and Other Applications: A Review," Renewable Sustainable Energy Rev., **14**, pp. 217–232.
[13] Incropera, F., Dewitt, D., Bergman, T., and Lavine, A., 2007, *Fundamentals of Heat and Mass Transfer*, 6th ed., John Wiley & Sons, Washington, DC.
[14] Becker, E., 1994, *Microalgae Biotechnology and Microbiology*, Cambridge University Press, Cambridge.
[15] Bolton, J., and Hall, D., 1991, "The Maximum Efficiency of Photosynthesis," Photochem. Photobiol., **53**(4), pp. 545–548.
[16] Williams, D., 1991, "A Comparison of Spectral Reflectance Properties at the Needle, Branch, and Canopy Level for Selected Conifer Species," Remote Sens. Environ., **93**, pp. 35–79.
[17] Gueymard, C., 2004, "The Sun's Total and Spectral Irradiance for Solar Energy Applications and Solar Radiation Models," Sol. Energy, **76**(4), pp. 423–453.
[18] Irvine, W. M., and Pollack, J. B., 1968, "Infrared Optical Properties of Water and Ice Spheres," Icarus, **8**, pp. 324–360.
[19] Howell, J., and Siegel, R., 2002, *Thermal Radiation Heat Transfer*, 4th ed., Taylor & Francis, New York.
[20] Mills, A., 1999, *Heat Transfer*, 2nd ed., Prentice Hall, Upper Saddle River, NJ.
[21] Mills, A., 2001, *Mass Transfer*, 2nd ed., Prentice Hall, Upper Saddle River, NJ.
[22] Moran, M., and Shapiro, H., 2003, *Fundamentals of Engineering Thermodynamics*, 5th ed., John Wiley & Sons, New York.
[23] Duffie, J., and Beckman, W., 2006, *Solar Engineering of Thermal Processes*, 3rd ed., John Wiley & Sons, Hoboken, NJ.
[24] Berberoglu, H., Pilon, L., and Melis, A., 2008, "Radiation Characteristics of *Chlamydomonas reinhardtii* CC125 and Its Truncated Chlorophyll Antenna Transformants *tla1, tlaX* and *tla1-CW+*," Int. J. Hydrogen Energy, **33**(22), pp. 6467–6483.
[25] Wilcox, S., and Marion, W., 2008, "Users Manual for TMY3 Data Sets," National Renewable Energy Laboratory, Golden, CO, Technical Report No. NREL/TP-581-43156.